آشکار سازی فوتون‌های فرابنفش خورشید-کور با استفاده از نانونوارهای آرمچیر گرافن و سورس ودرین نامتقارن

فاطمه استواری[۱] و محمد کاظم مروج فرشی[۲]

[۱]دانشکده فیزیک دانشگاه تربیت مدرس، بلوار آل احمد، تهران
[۲] گروه الکترونیک، دانشکده مهندسی برق و کامپیوتر، دانشگاه تربیت مدرس، بلوار آل احمد، تهران

چکیده – مشخصات آشکارسازهای نوری متشکل از کانال‌هایی از جنس نانو نوار گرافن آرمچر و ا الکترودهای سورس و درین نامتقارن، در معرض تابش فوتون هایی در گستره‌ی انرژی فروسرخ میانه تا فرابنفش خورشید-کور شبیه‌سازی شده‌است. شبیه‌سازی نشان می‌دهد درغیاب بایاس خارجی، بیشینه‌ی جریان نوری برای افزاره‌ای که سورس و درین نامتقارن آن از اتصال‌های Au/G و Ti/G تشکیل شده‌اند، به‌ازای تابشی با انرژی و شدت ورودی $5/02\ eV$ و $10^3\ W\cdot cm^2$ برابر $1/897\ \mu A$ است. در این شرایط بازدهی کوانتومی ٪۶۰ و پاسخ‌دهی اپتیکی آشکارساز $A\cdot mW^{-1}$ ۱۳/۴ است. تغییرات جریان موضعی در طول کانال و تغییرات جریان کل بر حسب ولتاژ گیت بیانگر تغییرپلاریتی جریان با عبور از نقطه دیراک است. همچنین جریان نوری باعث جابجایی منفی در جریان خواهد شد. شبیه‌سازی ها با بهره‌گیری از حل همزمان معادله‌ی گرین غیر تعادلی با معادله پواسن انجام شده است.

کلید واژه- آشکارساز نوری، بازدهی کوانتومی، تابع گرین غیر تعادلی، جریان نوری، نانو نوار گرافن

Solar Blind Ultraviolet Photodetection with Armchair Graphene Nanoribbons and Asymmetric Source and Drain Contacts

Fatemeh Ostovari[1] and Mohammad Kazem Moravvej-Farshi[2]
[1] Department of Physics, Tarbiat Modares University, P.O. Box14115-335, Tehran 1411713116, Iran
[2] Faculty of electrical and Computer Engineering, advanced Devices Simulation Lab (ADSL), P. O. Box 14115-194, Tehran 1411713116, Iran

Abstract-Characteristics of photodetectors consisting armchair graphene nanoribbons (a-GNR) channels and asymmetric source and drain contacts, under monochromatic illuminations of various incident energies in the range of mid infrared to solar blind ultra violet, are simulated. Simulations show, for light of incident intensity 10^3 W/cm,^{2}the photocurrent spectrum in the device with asymmetric leads made of Au- and Ti-contacted graphenes, under no external bias, exhibits a peak of 1.897 μA, at the energy E=5.02 eV. This peak corresponds to the quantum efficiency of 60% and the detection responsivity of 13.4 $A\cdot mW^{-1}$. Polarities of the local photocurrents alter when the gate-source voltage approaches to the Dirac point, for which the maximum total photocurrent is achieved. Finally, the total device current versus the drain-source voltages obtained under monochromatic illumination, for V_{GS}=0, is shown to shift toward negative values in comparison to the dark current. Simulations are performed, using the nonequilibrium Green's function (NEGF) formalism coupled to the Poisson solver.

Keywords: photodetector; graphene nanoribbon (GNR); nonequilibrium Green's function (NEGF); photocurrent; quantum efficiency

Solar Blind Ultraviolet Photodetection with Armchair Graphene Nanoribbons and Asymmetric Source and Drain Contacts

Fatemeh Ostovari, Mohammad Kazem Moravvej-Farshi
Fatemeh.ostowary@modares.ac.ir; farshi_k@modares.ac.ir

1 Introduction

Optical and electrical properties of graphene nanoribbons (GNRs) make them promising materials for variety of optoelectronics applications [1]. Recent experiments on photocurrent generation have shown that in the vicinity of the metal/graphene interfaces, where charge inhomogeneities are induced, photoresponses are strong. So, properties of the source/drain metal contacts play an important role in the magnitude of photocurrent, in the absence of any external bias, because of the weak built-in electric field in the graphene channel [2, 3]. This is only possible when the scattering lengths are long and the carrier transport is ballistics throughout the channel. The larger the difference between the source and drain metals work functions the larger the built-in field and so is the photocurrent through the external circuit. Graphene absorption is limited to infrared wavelengths [4]. Nonetheless, GNR-based photodetectors can operate down to ultraviolet wavelengths due to their band gap tunability. However, to the best of our knowledge, characteristics of GNR-based photodetectors with asymmetric source and drain contacts have not been reported in the literature, so far. In this paper, we report the results of our numerical studies on such photodetectors that can operate at deep ultraviolet wavelengths, with high quantum efficiency at zero source-drain and gate voltages.

2 Asymmetric contacts and the built-in potential

Figure 1(a) shows the schematic representation of a photodetector with an armchair GNR (a-GNR) channel and asymmetric source and drain contacts, under the illumination of a monochromatic light. The a-GNR channel is assumed to be thirty unit-cells long (i.e. $L_{ch} \approx 12.709$ nm) and ten C-atoms wide (i.e. $W_{ch} \approx 1.11$ nm). Experimental and theoretical studies have consistently demonstrated that when graphene of work function Φ_G (4.5 eV) contacted to metal of work function Φ_M, the chemical adsorption (metal doping) on graphene imparts a shift of ΔE_F in the graphene Fermi level [2, 3]. This shift for metals like Au, Pd, and Ti with work functions Φ_M= 4.7, 4.65, and 4.3, respectively, equals 250, 170, and −230 meV. In other words, Au and Pd make the underneath

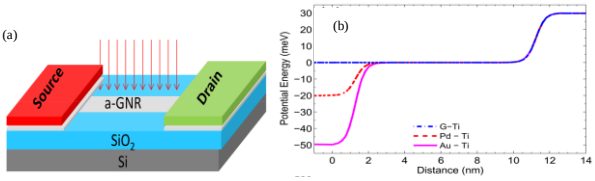

Fig. 1:(a) Schematic representation of a photodetector with an a-GNR channel and asymmetric source and drain contacts, (b) The potential energy profiles across the a-GNR channel connected between three asymmetric source (G, Pd, and Au) and drain (Ti) contacts.

graphene p-type and Ti makes it n-type. As a consequence of these shifts, the potential steps between the metal-contacted graphene lead and the Dirac point in the a-GNR channel becomes [2,3]:

$$\Delta V\,(\mathrm{eV}) = \Phi - \Delta E - \Phi_G \pm 0.0263\, V_{GS} - eV_{GS} \qquad (1)$$

wherein (+) and (−) correspond to the sign of the gate to source bias (V_{GS}) with respect to the Dirac point and e is the electron charge. For V_{GS}=0, potential steps for Au/G, Pd/G, and Ti/G leads are ΔV=−50, −20, and 30 eV respectively.

Employing Poisson solver, we have evaluated the profiles of potentials across the channel, for two cases in which the drain leads are all made of Ti/G and the source electrodes are made of, Pd/G (dashes), and Au/G (solid curve), and compared them with a case in which the source graphene has no metal contact on it (Fig 1.b).

3 Simulation method

Assuming the nearest neighbor tight binding approximation and use of the self-consistent non-equilibrium Green's function (NEGF) formalism for ballistic transport leads to the photocurrent spectrum, across the device [5]:

$$I_{ph}(E) = \left(\frac{2ei}{h}\right)\mathrm{Tr}[H_{k,k+1}G^n_{k,k+1}(E) - H_{k+1,k}G^n_{k+1,k}(E)] \qquad (2)$$

where i, k and h are the imaginary unit, position of atom in channel and the Planck's constant, respectively. H, and G^n are the Hamiltonian and the electrons correlation function:

$$G^n(E) = G(E)[\Gamma_S(E) f_S(E) + \Gamma_D(E) f_D(E) + \Sigma_{ph}]G^\dagger(E) \qquad (3)$$

where $f_{S/D}$ is the source/drain lead Fermi–Dirac function, $\Gamma_{S/D}$ represents the broadening function due to the coupling of the source (drain) lead to the channel, G and $G^\dagger$ represent the Green function and its adjoint, and Σ_{ph} is the photon self-energy that is related to electron-photon scattering

rate and is determined by the incident light intensity, I_ω (E). One of the key parameter for a photodetector is its quantum efficiency ($\eta \equiv EI_{\rm ph}/e(L_{\rm ch}\times W_{\rm ch})I_\omega$) that is defined as the number of photogenerated carriers that contribute to the current flowing through the external circuit divided by the number of the monochromatic incident photons.

Another important parameter for a photodetector is its responsivity that is defined as the ratio of the output photocurrent to the incident photons power – i.e., $I_{\rm ph}/P_{in} \equiv I_{\rm ph}/(L_{\rm ch}\times W_{\rm ch})I_\omega$

Moreover, a vital characteristic for a photodetector that can vary with the externally applied biases and also with the incident light intensity is its dark current [5]:

$$I_{\rm dark} = \frac{q}{h}\int T(E)\left[f_S(E) - f_D(E)\right]dE \qquad (4)$$

4 Simulation results and discussion

Assuming normal monochromatic illumination of constant intensity I_ω=10^3 W/cm^2, we have spanned the photon energy (E) over a wide range mid IR to far solar blind UV region (0.1 eV ≤ E ≤ 10 eV), and simulated the device photocurrent and quantum efficiency, with no external biases. In these simulations the substrate effect on the channel has been neglected. Figure 2 illustrates the simulated photocurrent spectrums (a) and the corresponding quantum efficiency (b) for the three photodetector structures. The dots-dashes, dashes, and solid curves represent the spectra for the device having the source terminals made of G, Pd/G, and Au/G, respectively. As can be observed from Fig. 2(a), each photocurrent spectrum exhibits seven peaks in the given energy range that correspond to the allowed transitions between the valence states and conduction states of the a-GNR channel. However, each spectrum has one

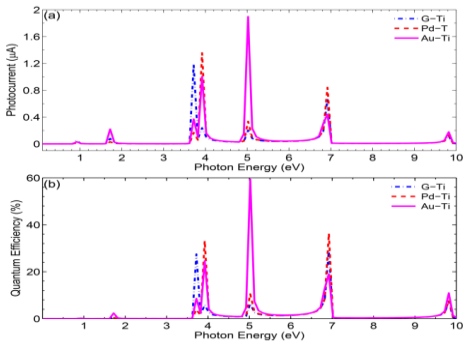

Fig. 2: (a) Photocurrent and (b) quantum efficiency of the three photodetectors with asymmetric source drain electrodes, under no external applied biases, versus the incident photon energy.

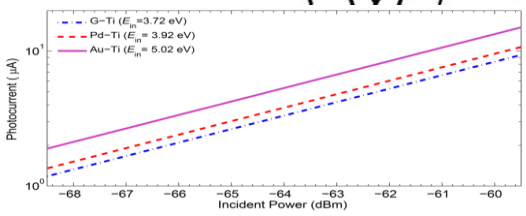

Figure 3: Photocurrent versus incident optical power for photodetectors with asymmetric source-drain contacts, under no external biases.

peak that corresponds to the most probable transition at a particular energy. Similar peaks can be observed in the quantum efficiency spectrums shown in Fig. 2(b), as expected.

The photon energies at which the most probable transitions corresponding to the peak in the quantum efficiency, for the photodetectors whose source electrodes are made of G, Pd/G, and Au/G, equal 3.72, 3.92, and 5.02 eV, respectively.

Next, for each of the three photodetectors, we have assumed a single monochromatic illumination of energy at which corresponding photocurrent spectrum has the largest peak, and varied its flux intensity in the range of $10^3 \le I_\omega \le 10^4$ W/cm^2 and calculated the photocurrent flowing out of the drain contact.

Figure 3 illustrates the $I_{\rm ph}$-$P_{\rm in}$ (dBm) plots, for the three given photodetectors. The responsivities corresponding to asymmetric source leads G-Ti, Pd-Ti, and Au-Ti that are represented, respectively, by dots-dashes, dashes, and solid curve are 10.4, 11.9 and 13.4 (AmW^{-1}), respectively.

Now, we investigate the effect of the applied gate voltage on the local and total photocurrent throughout the a-GNR channel for the device, with asymmetric source (Au/G) and drain (Ti/G)

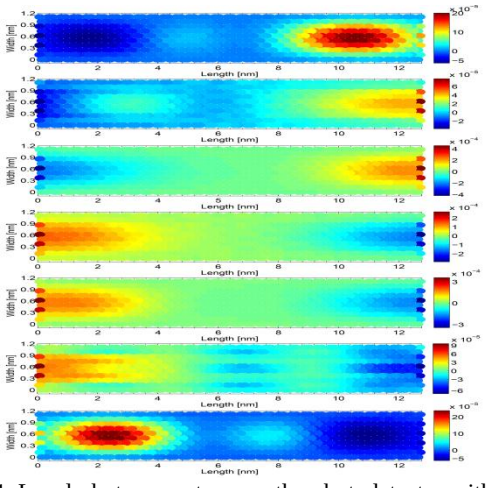

Fig. 4: Local photocurrent across the photodetector with Au-Ti leads under biasing conditions of V_{DS}=0 and V_{GS}= (a) −80 mV, , (b) −40 mV, (c) −20 mV, (d) 0, (e) 20 mV, (f) 40 mV and (g) 80 mV. Color bars indicate the local currents in units of μA.

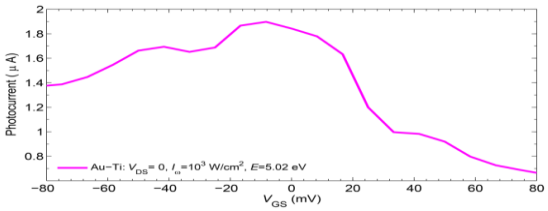

Fig. 5: Total photocurrent versus the gate to source voltage, across the photodetector with asymmetric source (Au/G) and drain (Ti/G) leads under monochromatic illumination of incident intensity 10^3 W/cm^2 and energy 5.02 eV, for *V*DS=0.

leads, when under illumination of a mono-chromatic incident light beam of intensity 10^3 W/cm^2 and energy 5.02 eV and for V_{DS}=0. The color bars indicate the local photocurrents in units of μA. As can be observed from all cases depicted in Fig. 4, the photocurrents are localized around the points inside the channel near the source and drain terminals, as expected. For V_{GS}=−80 mV the local current intensity is negative around the source (p-type regime) and positive near the drain (n-type regime). As V_{GS} becomes more positive, the local current intensities near the source and drain regions both decrease, until they change polarities around the Dirac point, for which the total photocurrent maxima occurs. Figure 5 illustrates the total photocurrent, for the device with asymmetric source (Au/G) and drain (Ti/G) leads, versus V_{GS}. Other conditions are the same as those for Fig.4. As can be observed from this figure the maximum current, for this device under the given conditions, occurs around the Dirac point, which is in accordance to the change of polarities observed for the local currents.

Figure 6 depicts the dark current (dots-dashes) versus the external bias applied between the source and drain leads (V_{DS}), for V_{GS}=0.

This figure also compares the dark current with I_D-V_{DS} characteristics of the device under monochromatic illumination of incident intensities 10^3 and 5×10^3 W/cm^2. As can be observed from this figure, the I_D-V_{DS} curves under illumination are shifted toward negative current values, with respect to the dark current. This is because; the dark current and the photocurrent are in opposite directions.

5 Conclusion

Assuming the nearest neighbor tight binding approximation and employing the self-consistent non-equilibrium Green's function (NEGF) form-alism for ballistic transport we have numerically simulated the photocurrents and quantum efficiencies of photodetectors having a-GNR channels of 12.709 nm long and 1.11 nm wide with asymmetric source and drain contacts versus energies of the monochromatic illuminations of fixed incident intensities of 1 kW/cm^2. The n-type drain electrodes for all three

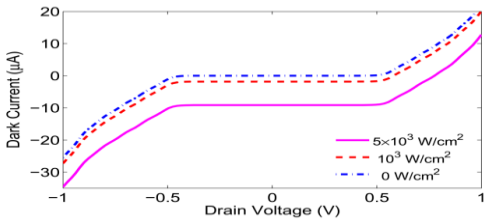

Fig.6. Dark current with and without illumination of 5.02 eV photon vs drain voltage at zero gate voltage in Au- Ti contacted device.

devices are assumed to be made of Ti-contacted graphenes (Ti/G), while the source electrodes for two of the three are assumed to be p-type made of Au-contacted and Pd-contacted graphenes (Au/G and Pd/G, respect-tively). The source electrode for the third device is assumed to graphene with no metals on the top. Simulations show the photocurrent spectrum for the aforementioned photodetectors, obtained in absence of any external biases applied to the device terminals, exhibit their highest peak currents of 1.183, 1.355, and 1.897 μA at E=3.72, 3.92, and 5.02 eV, respectively. The corresponding, quantum efficiencies are found to be ~27.5, 33.2 and 59.5%, respectively. Responsivities for these three photodetectors under monochromatic illuminations at aforemen-tioned energies and zero applied biases are found to be 10.4, 11.9, and 13.4 A/mW. Simulations also show that the peak in the total photocurrent versus the gate-source voltages occur near the Dirac point for which the local photocurrents across the channels change polarities. Moreover, comparison of the total device current versus the drain source voltages obtained under monochromatic illumi-nation and for V_{GS}=0, with the dark current obtained under the same biasing conditions has shown that former shifts toward the negative current values because the dark current and photo currents flow in the opposite directions.

References

[1] F. Bonaccorso *et.al*, "Graphene photonics and opto-electronics," *Nat. Photonics.* Vol. 4**,** pp. 611–622, 2010.

[2] F. N. Xia *et.al*, Bonaccorso et.al, "Ultrafast graphene photodetector" *Nat. Nanotechnol.* Vol. 4**,** pp. 839–843, 2009.

[3] E. J. H. Lee *et.al*, "Contact and edge effects in graphene devices" *Nat. Nanotechnol.* Vol. 3**,** pp. 486–4902, 2008.

[4] K. Fai Mak *et.al*, "Optical spectroscopy of graphene: From the far infrared to the ultraviolet" *Solid State Communications*. Vol. 152**,** pp.1341–1349, 2012.

[5] S. Datta, "Nanoscale device modeling: the Green's function method" *Superlattices and Microstructures*. Vol. 28**,** pp. 256–278, 2000.